



Wear Modelling of the Thread Pair in a Planetary Roller Screw Mechanism

Shangjun Ma²(✉), Qianjin Xu¹, Chuangchuang Li¹, Jianxin Zhang^{1,3}, and Geng Liu^{1,2}

¹ Shaanxi Engineering Laboratory for Transmissions and Controls, Northwestern Polytechnical University, Xi'an, China

² Xi'an Ding Bai Precision Technology Co., Ltd., Xi'an 710000, China
mashangjun@nwpu.edu.cn

³ Jiangshan Heavy Industries Research Institute Co., Ltd., Xiangyang 441057, China

Abstract. Based on the contact characteristics of helical surfaces and the coexistence of rolling and sliding at the screw-roller interface, a forecast model of the thread pair using Archard wear theory is proposed. To obtain the wear depth and the wear volume of the screw raceway in the whole effective stroke, a test rig of the thread wear is developed to obtain the wear rate that can be used to fit the values of the stress index and speed index. The area coefficient is further deduced to reflect the real wear condition. The calculation method of the relative sliding speed, coordinate transformation and load distribution are provided, the finite element (FE) model is established, and the transient dynamic simulation of the thread wear is implemented to verify the correctness of the wear model. The relative error is less than 9% between the FE model and proposed model by comparing the wear depths and wear volumes, which indicates the wear model proposed in this paper is valid and can be used to forecast the thread wear of the PRSM. Finally, the wear behavior of the thread pair is preliminarily discussed based on the FE model.

Keywords: Planetary roller screw · Adhesive wear · Simulation analysis · Wear depth · Sliding wear

1 Introduction

The planetary roller screw mechanism (PRSM) is a mechanical transmission device used to convert rotary motion into linear motion (as shown in Fig. 1). It provides more contact points than for the same size of ball screw mechanism. The PRSM has a higher stiffness, a higher load capacity and 15 times the travel life of similarly sized ball screw. These advantages make it a suitable device for feed-drive applications. In addition, the PRSM offers a perfect replacement for hydraulics because of its load and cycle capability [1]. Recently, increasing demands in precision engineering applications for positioning systems have instigated research into the PRSM as it can be involved in electromechanical actuators developed for all electric aircraft [2], thrust vector control [3] and ship engineering [4].

As shown in Fig. 1, the principle components of the PRSM are screw, nut and equally spaced rollers. The screw and nut with a multistart straight-shaped thread provide a

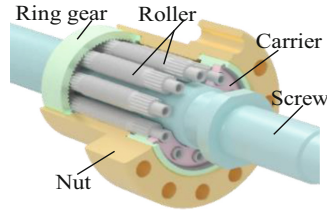


Fig. 1. The planetary roller screw mechanism

helical raceway for the multiple rollers, and the roller is a singlestart rounded-shaped thread that provides better contact characteristics. The rollers are rolling elements of the PRSM and have small thread height and pitch to engage with the screw and nut threads. Their threads are manufactured with a rounded half section to enhance the contact characteristics. Such a robust design is particularly well suited for applications that require very high positional accuracy, high loads and high speeds.

In the wear research of the thread transmissions, Aurégan et al. [5] investigated the tribological behavior of a thread pair, and wear tests were performed on a rolling-sliding test rig. The results reveal that adhesive wear occurrence is strongly influenced by rolling speed and normal load. They also studied the tribological behavior of helical surfaces with hard coatings. The wear state of hard coatings was further studied under different working conditions, and the two damage modes were identified [6]. Xie et al. [7] established a mixed lubrication model considering parameters such as contact load, thread geometry and surface roughness. Zhou et al. [8] calculated the sliding velocity of the contact point in PRSM, and studied the lubrication characteristics and transient behavior of the PRSM based on the transient mixed elastohydrodynamic lubrication model.

In the study of contact characteristics, rolling-sliding and load distributions are related to wear. Sandu et al. [9] established a general model of the thread profile that can be used to calculate the geometric profile of the threads with various configurations and optimized thread profile parameters were obtained based on the model. Then, Sandu et al. [10] deduced the calculation formula of the principal curvature of the helical surface, presented the calculation method of the size, geometry and orientation of the contact ellipse, and studied the kinematic characteristics of the local contact area. According to the characteristics of helical surfaces of screw, rollers and nut, Qiao et al. [11] established a general profile equation and helical surface equation of components in a normal section, modified the calculation method of principal curvature and analyzed the contact characteristics. Velinsky et al. [12] presented a kinematic model to reveal that there is always slip between the screw and the roller in the axial direction. Furthermore, Jones et al. [13] developed a kinematic model to predict the axial migration of rollers with respect to nut in the PRSM. Ma et al. [14] studied the rolling-sliding characteristics by calculating the relative velocities of contact points on screw-roller and nut-roller interfaces, and the nut side, and the influence of the contact angle, helix angle and thread number of the roller on sliding-rolling ratios was considered. Abevi et al. [15] presented a hybrid model using the bar, beam, and nonlinear spring elements to compute the load

distribution and axial stiffness of the PRSM. Zhang et al. [16] proposed a model to calculate load distributions over PRSM threads with pitch deviation, the influence of pitch deviation on load distributions can be verified by comparing wear depths.

The existing research provides a theoretical basis for the modelling and analysis of the thread wear. However, when the PRSM accelerates or decelerates, frictional heat will result in the deterioration of lubrication, which will further lead to wear at the contact area in the PRSM. Wear can increase the clearance of meshing threads and decrease the PRSM's transmission performance and lifespan. At present, research on wear mainly focuses on experimental research, and few researchers have proposed models to investigate the wear behavior of the PRSM. In addition, the PRSM is a closed system, and it is difficult to study wear when it is directly moving, especially multiple threads with different contact conditions. Therefore, this paper provides a fundamental examination of the thread wear based on the rolling and sliding at the screw-roller interface. First, in Sect. 2, a new wear model is developed based on adhesive wear theory. Second, a test rig of the thread wear is developed to obtain the wear rate that can be used to fit the stress index and speed index. Third, the calculation method of the relative sliding speed, coordinate transformation and load distribution are provided. To verify the correctness of the wear model, the FE model is established, and the transient dynamic simulation of the thread wear is implemented in Sect. 3. Finally, the correctness of the model is verified by comparing the wear depth and wear volume calculated by the FE model.

2 Modelling

2.1 Modelling of Wear

The accuracy loss of the PRSM is mainly caused by the wear. The wear types of the PRSM mainly include contact fatigue wear and adhesive wear. The contact fatigue wear mainly reflects the fatigue damage in the thread raceway, which is usually used to predict the service life. The adhesive wear is the main factor leading to accuracy degradation. Because the helix angle of the roller thread is equal to that of the nut thread and the gear teeth at both ends of the roller mesh with the internal gear ring, pure rolling between the roller and the nut can be ensured. In contrast, the sliding exists at the screw-roller interface [12]. The motion characteristic of the coexistence of rolling and sliding is the main cause of wear. Therefore, the wear at the screw-roller interface is focused in this paper.

In the PRSM, the hardness of the screw raceway (54–60 HRC) is lower than that of the roller (60–64 HRC), which means that the screw raceway is prone to the adhesive wear. Based on Archard wear theory, under the normal load N_i , the normal wear depth of the contact position between the i th roller thread and screw raceway can be expressed as:

$$\Delta\delta_i = \frac{W_i}{A_i} = K \frac{N_i}{\pi H a_i b_i} v t \quad (1)$$

where W_i is the wear volume, A_i is the contact area, K is a dimensionless wear constant, H is the hardness of the softer material, v is the relative sliding speed between the roller

thread and screw raceway, t is the wear time, a_i is the semimajor axis of the contact ellipse, and b_i is the semiminor axis of the contact ellipse.

The contact stress P_i at the contact point between the i th roller thread and the screw raceway can be written as:

$$P_i = \frac{N_i}{A_i} = \frac{N_i}{\pi a_i b_i} \quad (2)$$

Substituting Eq. (2) into Eq. (1) yields the following form:

$$\Delta\delta_i = K \frac{P_i v}{H} t \quad (3)$$

Generally, the relationships between wear and that stress and between wear and sliding speed are nonlinear. Considering the influence of sliding speed and contact stress on the wear process, the stress index m and speed index n are introduced to modify Eq. (3). Thus, Eq. (3) can be modified as [17]:

$$\Delta\delta_i = K \frac{P_i^m v^n}{H} t \quad (4)$$

For the PRSM, the wear principle of the roller thread and screw raceway is shown in Fig. 2. As shown in Fig. 2, L_S is the effective stroke of the screw thread, and L_{RS} is the thread raceway length corresponding to the effective stroke of the screw and also the total length of the corresponding wear area. In traditional Archard wear theory, the two relative sliding contact surfaces are always in contact. However, for the point contact of helical surfaces in the PRSM, the screw thread raceway can not participate in wear at any time, and the wear area is only the contact ellipse area, as shown in Fig. 2. Therefore, the traditional Archard wear model cannot be directly used to analyze the wear of the PRSM. It is necessary to consider the local contact of the threads and establish a new mathematical model of the thread wear. To more accurately calculate the wear depth and the wear volume of the screw raceway in the whole effective stroke, based on Eq. (4), this paper uses the experimental method to obtain the values of m and n and further deduces the area coefficient f_r to reflect the real wear of the roller thread and the screw raceway in the PRSM.

Figure 3 shows the actual wear diagram of the screw raceway. The cross section of the wear area can be approximately regarded as an elliptical arc. The maximum wear depth is h_0 , the wear width is $2a$, and a is the semimajor axis of the contact ellipse. The total length of the wear area is the thread raceway length L_{RS} corresponding to the effective stroke of the screw.

The wear depth h at different section positions can be approximated as:

$$h = h_0 \sqrt{1 - \left(\frac{x}{a}\right)^2} \quad (5)$$

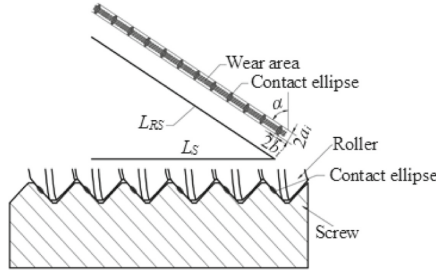


Fig. 2. The wear principle of roller thread and screw raceway

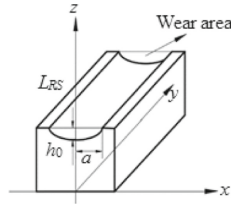


Fig. 3. The actual wear diagram of screw raceway

Then, the wear cross-sectional area can be represented as:

$$S = \int_{-a}^a h_0 \sqrt{1 - \left(\frac{x}{a}\right)^2} dx \quad (6)$$

The total wear volume can be expressed as:

$$W = L_{RS} \int_{-a}^a h_0 \sqrt{1 - \left(\frac{x}{a}\right)^2} dx = \frac{\pi a h_0 L_{RS}}{2} \quad (7)$$

When the actual wear of the screw raceway is not considered, the wear volume is expressed as:

$$W = \pi a b \Delta \delta_i \quad (8)$$

Combining Eqs. (7) and (8) result in the following expression:

$$h_0 = \frac{2b}{L_{RS}} \Delta \delta_i \quad (9)$$

Therefore, the area coefficient f_r of the i th contact ellipse is expressed as:

$$f_r = \frac{2b_i}{L_{RS}} = \frac{2b_i}{n_S L_S / \sin \alpha_S} \quad (10)$$

where n_S is the number of the thread raceways of screw thread, α_S is the helix angle of the screw thread and b_i is the semiminor axis of the i th contact ellipse.

Combining Eqs. (4) and (10), the wear depth of the contact area between the i th roller thread and the screw raceway can be represented as:

$$\Delta\delta_i^{\text{new}} = f_r \Delta\delta_i = 2K \frac{b_i P_i^m v^n t}{n_S L_S H} \sin \alpha_S \quad (11)$$

According to Fig. 3 and combining Eqs. (4) and (9), the normal wear volume between the i th roller thread and the screw raceway can be written as

$$W_i = \frac{\pi a_i h_0 L_{RS}}{2} = K \frac{\pi a_i b_i p_i^m v^n t}{H} \quad (12)$$

If the number of roller threads meshed with the screw thread is τ , the normal wear volume of a single roller on the screw raceway can be expressed as:

$$W_i^{\text{roller}} = \sum_{i=1}^{\tau} K \frac{\pi a_i b_i p_i^m v^n t}{H} \quad (13)$$

Similarly, assuming that each roller carries the same load, when k rollers are meshed with the screw raceway, the total normal wear volume of the PRSM can be expressed as:

$$W_i^{\text{PRSM}} = k \sum_{i=1}^{\tau} K \frac{\pi a_i b_i p_i^m v^n t}{H} \quad (14)$$

2.2 Analysis of the Relative Velocity at the Screw-Roller Interface

The contact location between the screw and roller in the plane projection is shown in Fig. 6, where Q_{SR} is the contact point, r_{S_c} and $r_{R_{S_c}}$ are the radii to the contact point on the screw and roller, respectively, and φ_{S_c} and $\varphi_{R_{S_c}}$ are the contact deviation angles to the contact location on the screw and roller, respectively.

The kinematic relationship of the PRSM indicates that the contact point at the screw-roller interface is not on the central axis of the cross-sectional plane, while the roller-nut interface contact point lies on the central axis of the cross-sectional plane [18]. Therefore, to establish an accurate wear model, the relative velocity of the contact point is very important, and the relative velocity can be obtained by determined the velocity difference at the contact point between two contact surfaces. The relative positions of the components in the PRSM are shown in Fig. 4.

As shown in Fig. 3, the coordinate system of a component $o_S-x_S y_S z_S$ denotes the motion relationship of the screw relative to the fixed coordinate system $o-xyz$. The angular velocity of the screw is denoted as ω_S , the angular velocity of the roller is denoted as ω_R , and the roller's revolution angular velocity is denoted as ω_H .

P_{SR} is the contact point at the screw-roller interface, and the relative position of the screw and roller can be denoted with contact radii r_{SP} and r_{RPS} and contact deviation angles φ_{SP} and φ_{RPS} .

When the screw thread is meshed with the roller thread, the normal vectors of screw thread N_{SP} and roller thread N_{RPS} at the contact point P_{SR} can be written as [19]:

$$N_{SP} = \begin{bmatrix} \cos \varphi_{SP} \tan \beta_{SP} + \sin \varphi_{SP} \tan \lambda_{SP} \\ \sin \varphi_{SP} \tan \beta_{SP} - \cos \varphi_{SP} \tan \lambda_{SP} \\ 1 \end{bmatrix} U_S \quad (15)$$

$$N_{RPS} = \begin{bmatrix} -\cos \varphi_{RPS} \tan \beta_{RPS} - \sin \varphi_{RPS} \tan \lambda_{RPS} \\ \sin \varphi_{RPS} \tan \beta_{RPS} - \cos \varphi_{RPS} \tan \lambda_{RPS} \\ -1 \end{bmatrix} U_S \quad (16)$$

where β_{SP} and β_{RPS} are the flank angles of the screw thread and roller thread at contact point P_{SR} . λ_{SP} and λ_{RPS} are the helix angles of the screw thread and roller thread at contact point P_{SR} . U_S is the unit vector associated with the coordinate system of the screw.

The parameters λ_{SP} , λ_{RPS} and β_{RPS} in Eqs. (15) and (16) can be expressed as:

$$\tan \lambda_{SP} = L_S / (2\pi r_{SP}) \quad (17)$$

$$\tan \lambda_{RPS} = L_R / (2\pi r_{RPS}) \quad (18)$$

$$\tan \beta_{RPS} = \frac{r_{RPS} - r_R - u_T}{\sqrt{r_T^2 - (r_{RPS} - r_R - u_T)^2}} \quad (19)$$

where L_S and L_R are the leads of the screw and roller, respectively, r_R is the nominal radius of the roller, r_T is the profile radius of the roller thread and u_T is the coordinate of any point on the threaded surface.

According to the motion relationship of the components shown in Fig. 4, the velocity of contact point P_{SR} on the screw V_{SP} is calculated as follows:

$$V_{SP} = \begin{bmatrix} -r_{SP}\omega_S \sin(\varphi_{SP} + \theta_H) \\ r_{SP}\omega_S \cos(\varphi_{SP} + \theta_H) \\ 0 \end{bmatrix}^T U \quad (20)$$

where U is the unit vector associated with the fixed coordinate system $o-xyz$.

The velocity of contact point P_{SR} on the roller is then calculated as follows:

$$V_{RPS} = \begin{bmatrix} r_{RPS}\omega_R \sin(\varphi_{RPS} - \theta_H) - r_{SP}\omega_H \sin(\varphi_{SP} + \theta_H) \\ r_{RPS}\omega_R \cos(\varphi_{RPS} - \theta_H) + r_{SP}\omega_H \cos(\varphi_{SP} + \theta_H) \\ -\omega_S L_S / 2\pi \end{bmatrix}^T U \quad (21)$$

The velocity component of V_{SP} in the direction of the normal vector at contact point P_{SR} is given as:

$$V_{SP} \cdot N_{SP} = \frac{r_{SP}\omega_S \tan \lambda_{SP}}{\sqrt{1 + \tan^2 \lambda_{SP} + \tan^2 \beta_{SP}}} \quad (22)$$

Similarly, the velocity component of V_{RPS} in the direction of the normal vector at contact point P_{SR} is given as:

$$\begin{aligned} V_{RPS} \cdot N_{RPS} = & \\ & \frac{r_{RPS}\omega_R \tan \lambda_{RPS} - r_{SP}\omega_H \tan \lambda_{RPS} + \omega_S L_S / 2\pi}{\sqrt{1 + \tan^2 \lambda_{RPS} + \tan^2 \beta_{RPS}}} \end{aligned} \quad (23)$$

Based on the conditions of the principle of conjugate surfaces, that is: (1) the threaded surfaces must share a common normal vector at the contact point, and (2) the relative velocity of the screw and roller must be zero in the common normal direction at the contact point. Therefore, we can obtain $N_{SP} = -N_{RPS}$ and $V_{SP} \cdot N_{SP} = -V_{RPS} \cdot N_{RPS}$, which are given as:

$$\begin{aligned} & \frac{r_{SP}\omega_S \tan \lambda_{SP}}{\sqrt{1 + \tan^2 \lambda_{SP} + \tan^2 \beta_{SP}}} \\ = & \frac{r_{RPS}\omega_R \tan \lambda_{RPS} - r_{SP}\omega_H \tan \lambda_{SP} + \omega_S L_S / 2\pi}{\sqrt{1 + \tan^2 \lambda_{RPS} + \tan^2 \beta_{RPS}}} \end{aligned} \quad (24)$$

and

$$\frac{\omega_H}{\omega_R} = \frac{L_R}{L_S} \quad (25)$$

The leads of the roller and screw are given as:

$$L_R = p \quad (26)$$

$$L_S = n_{SP} \quad (27)$$

where p is the pitch of the thread and n_S is the number of starts of the screw thread.

Combining Eqs. (24)–(27), the relative velocity at the contact point P_{SR} between the screw and roller can be determined:

$$\begin{aligned} V_{SR} = V_{SR} - V_{RPS} \\ = \begin{bmatrix} -r_{SR}(\omega_S - \omega_H) \sin(\varphi_{SR} + \theta_H) - r_{RPS}\omega_R \sin(\varphi_{RPS} - \theta_H) \\ r_{SR}(\omega_S - \omega_H) \cos(\varphi_{SR} + \theta_H) - r_{RPS}\omega_R \cos(\varphi_{RPS} - \theta_H) \\ \frac{\omega_S L_S}{2\pi} \end{bmatrix}^T U \end{aligned} \quad (28)$$

As shown in Fig. 4, the wear occurs in the contact area, and the relative velocity of the contact point needs to be converted to the contact coordinate system, so that the relative speed components in the contact area can be obtained. Therefore, the contact coordinate system of the screw and roller needs to be established.

The contact coordinate systems of the components are shown in Fig. 5.

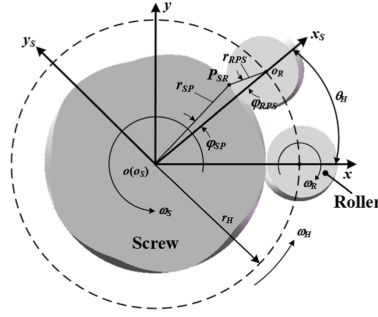


Fig. 4. Position relationships of the components

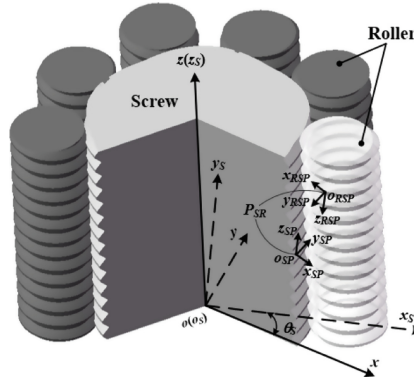


Fig. 5. The contact coordinate systems of the components

According to coordinate transformation, the relative velocity V_{SP} is transformed to the $o_{SP}-x_{SP}y_{SP}z_{SP}$ coordinate system by the following equations:

$$V_{SR} = \begin{bmatrix} -r_{SP}(\omega_S - \omega_H) \sin(\varphi_{SP} + \theta_H) - r_{RPS}\omega_R \sin(\varphi_{RPS} - \theta_H) \\ r_{SP}(\omega_S - \omega_H) \cos(\varphi_{SP} + \theta_H) - r_{RPS}\omega_R \cos(\varphi_{RPS} - \theta_H) \\ \frac{\omega_S L_S}{2\pi} \end{bmatrix}^T \quad (29)$$

$$\cdot M_U^{U_S^{-1}} M_{U_S}^{C_S^{-1}} U_{SP}$$

where U_{SP} is the unit vector associated with contact coordinate system $o_{SP}-x_{SP}y_{SP}z_{SP}$.

$$M_U^{U_S} = \begin{bmatrix} \cos \theta_S & \sin \theta_S & 0 \\ -\sin \theta_S & -\cos \theta_S & 0 \\ 0 & 0 & 1 \end{bmatrix}^T \quad (30)$$

$$M_{UN}^C = \begin{bmatrix} \frac{(\sin \theta_{NP} \tan \beta_{NP} - \cos \theta_{NP} \tan \lambda_{NP}) - \cos \theta_{NP}}{\sqrt{(1 + \tan^2 \lambda_{NP})(1 + \tan^2 \lambda_{NP} + \tan^2 \beta_{NP})}} & \frac{-\sin \theta_{NP}}{\sqrt{1 + \tan^2 \lambda_{NP}}} & \frac{\cos \theta_{NP} \tan \beta_{NP} + \sin \theta_{NP} \tan \lambda_{NP}}{\sqrt{(1 + \tan^2 \lambda_{NP} + \tan^2 \beta_{NP})}} \\ \frac{-(\cos \theta_{NP} \tan \beta_{NP} + \sin \theta_{NP} \tan \lambda_{NP}) \tan \lambda_{NP} + \sin \theta_{NP}}{\sqrt{(1 + \tan^2 \lambda_{NP})(1 + \tan^2 \lambda_{NP} + \tan^2 \beta_{NP})}} & \frac{\cos \theta_{NP}}{\sqrt{1 + \tan^2 \lambda_{NP}}} & \frac{\cos \theta_{NP} \tan \lambda_{NP} - \sin \theta_{NP} \tan \beta_{NP}}{\sqrt{(1 + \tan^2 \lambda_{NP} + \tan^2 \beta_{NP})}} \\ \frac{\tan \beta_{NP}}{\sqrt{(1 + \tan^2 \lambda_{NP})(1 + \tan^2 \lambda_{NP} + \tan^2 \beta_{NP})}} & \frac{\tan \lambda_{NP}}{\sqrt{1 + \tan^2 \lambda_{NP}}} & \frac{-1}{\sqrt{(1 + \tan^2 \lambda_{NP} + \tan^2 \beta_{NP})}} \end{bmatrix} \quad (31)$$

where θ_{SP} is the relative rotation angle of the screw and roller on the screw thread at the contact point.

2.3 Parameter Acquisition of the Stress Index and Speed Index

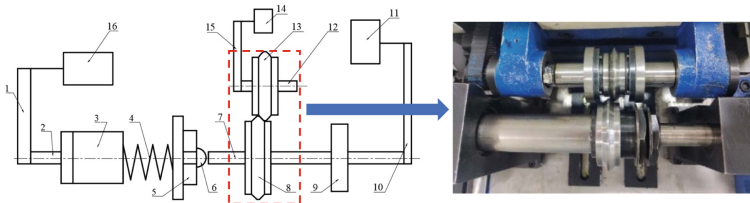
The experimental principle of wear test is shown in Fig. 6.

The difference in wear between the thread teeth of the planetary roller screw mechanism is only the difference in load distribution. Therefore, in order to simplify the experiment, only a pair of the thread teeth are made for the experiment. Since the helix angle will only affect the magnitude of the load and will not affect the position of the contact point and wear characteristics, and if the helix angle is considered, the test bench will be relatively large. In order to simplify the test bench, the test pieces processed in this paper do not consider the helix angle. In the follow-up study, we will further improve the experiment.

During the test, the relative sliding speed is controlled by adjusting the speed of screw drive shaft 7 and roller drive shaft 12. The axial force is applied by components such as loading motor 16, active loading screw 3 and loading spring 4 to simulate the loading on the thread pair. The torque sensor 9 is used to measure the friction torque of the thread pair under the given axial load and speed.

The main parameters of screw test piece 8 and roller test piece 13 are shown in Table 1.

In this paper, the bearing steel material is selected as the case. The screw material is 14NiCrMo, and the roller material is GCr15, whose density is $\rho = 7,810 \text{ kg/m}^3$, elastic modulus is $E = 212 \text{ GPa}$ and Poisson's ratio is $\mu = 0.29$. Before the test, the pieces are measured by a profilometer and precision electronic balance to obtain the thread profile size and weight for comparison after the wear test. To facilitate the thread wear test, a pair of the threads are used as the test object, and the helix angle of the thread is set

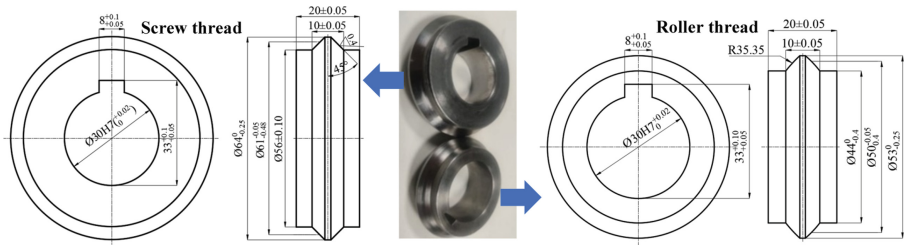


1 - Synchronous belt I; 2 - Active loading screw; 3 - Active loading nut; 4 - Loading spring; 5 - Axial force sensor; 6 - Centering steel ball by axial force; 7 - Screw drive shaft; 8 - Screw test piece; 9 - Torque sensor; 10 - Synchronous belt II; 11 - Screw drive motor I; 12 - Roller drive shaft; 13 - Roller test piece; 14 - Roller drive motor; 15 Synchronous belt III; 16 - Load motor

Fig. 6. Structure diagram of test rig of the thread wear

Table 1. The main parameters of tested pieces

Parameters	Screw thread	Roller thread
Flank angle β ($^{\circ}$)	45	45
Profile radius of the roller thread R (mm)	/	35.35
Thread thickness b (mm)	5	5
Roughness (μm)	0.06	0.29

**Fig. 7.** The pieces of the screw thread and roller thread**Table 2.** Test scheme under different loads

Axial load/N	Sample piece	Material	Angular velocity/rpm	Sliding-rolling ratio	Test time/min
100/200/300	Screw	14NiCrMo	300	0.3	300
	Roller	GCr15	271		

to zero; that is, the contact of a pair of the threads is simplified into two rings with a real profile, as shown in Fig. 7. Besides, the lubricant is applied only once on the thread surface to reduce the starting friction torque, and the thread wear will be in a dry friction state with the consumption of lubricating oil.

The test conditions are shown in Tables 2 and 3.

According to Sect. 2.1, the wear depth per unit time (i.e., wear rate) can be expressed as:

$$\frac{dh}{dt} = K \frac{P_i^m v^n}{H} \quad (32)$$

The contact stress P_i can be solved according to Hertz contact theory, the relevant calculation methods can be found in reference [19]. The helix angle is zero to ensure that the theoretical calculation is consistent with the test. The dimensionless wear constant K can be rewritten as:

$$K = \frac{H}{P_i^m v^n} \frac{dh}{dt} \quad (33)$$

Table 3. Test scheme under different angular speeds

Angular velocity/rpm	Sample piece	Material	Axial load/N	Sliding-rolling ratio	Test time/min
300	Screw	14NiCrMo	300	0.3	300
271	Roller	GCr15			
200	Screw	14NiCrMo			
181	Roller	GCr15			
100	Screw	14NiCrMo			
90	Roller	GCr15			

Table 4. The calculation results based on Hertz contact theory

Parameters	Axial load/N		
	100	200	300
a/mm	0.3508	0.4419	0.5059
b/mm	0.2355	0.2967	0.3396
A/mm^2	0.2595	0.4119	0.5398
σ_{max}/MPa	817.5	1029.9	1179.1

The relative sliding speed of tested pieces v is easily derived as:

$$v = v_{Screw} - v_{Roller} = \pi(n_{Screw}d_S - n_{Roller}d_R) \tag{34}$$

where n_{Screw} and n_{Roller} are the angular speed of the screw and the roller, respectively, and d_S and d_R are the nominal diameters of the screw thread and the roller thread.

Based on the parameters shown in Table 1, the results of the contact parameters calculated according to Hertz theory are shown in Table 4.

The wear amount is expressed by the mass difference before and after the test. Before each measurement, the test piece must be strictly cleaned and weighed after drying. After the wear mass is measured, it can be determined by the material density ρ to calculate the wear volume, i.e.

$$V = \frac{M}{\rho} \tag{35}$$

where M is the measured wear amount, $M = M_0 - M_1$, M_0 is the mass before the test, and M_1 is the mass after the test.

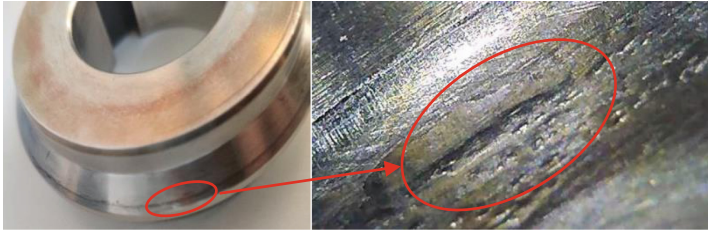


Fig. 8. The wear of the screw thread (14NiCrMo)

Table 5. The wear rate under different axial loads at 300 rpm

Axial load/N	100	200	300
Wear rate/(mm/s)	1.94×10^{-5}	2.36×10^{-5}	2.68×10^{-5}

Table 6. The wear rate under different angular velocities at 300 N

Angular velocity of the screw/(rpm)	100	200	300
Wear rate/(mm/s)	6.89×10^{-6}	1.39×10^{-5}	2.68×10^{-5}

The wear rate can be described as:

$$\frac{dh}{dt} = \frac{dV}{dAdt} \quad (36)$$

The screw test piece after the wear test is shown in Fig. 8.

The wear rate is calculated according to the wear amount, and the wear rate under different axial loads at 300 rpm (screw angular velocity) can be obtained, as shown in Table 5.

Similarly, the wear rate under different angular velocities at 300 N can be obtained, as shown in Table 6.

The stress index m and velocity index n are obtained by fitting the wear rate obtained from the test (Table 4 and Table 5). Then, the dimensionless wear constant K is calculated from Eq. (33). The fitting results are $m = 0.723$ and $n = 1.237$. The value range of the dimensionless wear constant K at different angular velocities and is ranged between 8.76×10^{-8} – 1.02×10^{-7} under different loads.

2.4 Load Distribution of the Threads

The load distribution on the thread can be obtained by the deformation coordination relationship between the screw-roller and nut-roller interfaces. The following equations can be used to calculate the load distribution, and the detailed calculation method can be found in references [15, 16].

$$\frac{\sum_{j=1}^i F_{SRj}}{k_{SB}} + \frac{F_{SRi} - F_{SRi+1}}{k_{ST}} + \frac{F_{SRi} + F_{SRi+1}}{k_{RSC}} \quad (37)$$

$$-\frac{\sum_{j=1}^i F_{SRj} - \sum_{j=1}^i F_{NRj}}{k_{RB}} - \frac{F_{SRi+1} - F_{SRi}}{k_{RT}} = 0$$

$$\frac{\sum_{j=1}^i F_{NRj}}{k_{NB}} + \frac{F_{NRi} - F_{NRi+1}}{k_{NT}} + \frac{F_{NRi} + F_{NRi+1}}{k_{RNC}} \quad (38)$$

$$-\frac{\sum_{j=1}^i F_{SRj} - \sum_{j=1}^i F_{NRj}}{k_{RB}} - \frac{F_{NRi+1} - F_{NRi}}{k_{RT}} = 0$$

where k_{SB} , k_{NB} and k_{RB} are the shaft section stiffness of the screw, nut and roller, respectively; k_{RSC} and k_{RNC} are the contact stiffnesses at the screw-roller interface and nut-roller interface, respectively; and k_{ST} , k_{NT} and k_{RT} are the thread stiffnesses of the screw thread, nut thread and roller thread, respectively.

According to Eqs. (37) and (38), the axial load F_{SRi} of each pair of contact threads of the screw and roller can be calculated. The ellipse parameters and contact ellipse area at the contact point can be obtained based on the Hertz contact theory.

3 Model Validation

3.1 Numerical Model Based on the FE Method

To verify the correctness of the wear model, the FE method is used for transient dynamic simulation of the thread wear. The contact pairs are created and assembled through the SolidWorks 2016, and the 3D FE model is developed using the ANSYS Workbench 19.2. Since the FE wear analysis is highly nonlinear and requires a long time for iterative calculation, it is assumed that the wear of the thread pair is uniform, and a section of the thread is taken for wear calculation. According to the parameters of the thread pair listed in Table 1, the contact model of the thread pairs at the screw-roller interface is established, as shown in Figs. 9 and 10. Meshing is based on the 10-node tetrahedral solid element 187. The contact model of the thread pair has 467,999 elements and 90,244 nodes. The material parameters of the screw thread and roller thread are consistent with those described in Sect. 2.3.

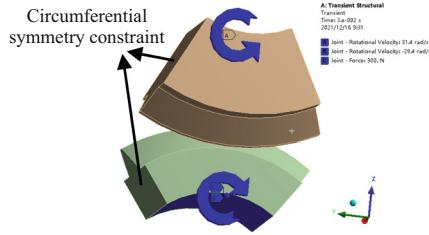


Fig. 9. The 3D model of the thread pair

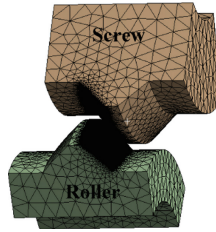


Fig. 10. The 3D FE model of the thread pair

The mechanical constraints are as follows: Fan-shaped end faces on both sides are a circumferential symmetry constraint based on the cyclic symmetric structure. The rotational freedom around the x -axis and the displacement freedom along the x -direction of the roller are released. The rotational freedom of the screw around the x -axis is released, the axial load applied on the roller thread along the x -axis is 300 N, and the angular velocity of the screw is 300 rpm, as shown in Fig. 9. The augmented Lagrange algorithm is adopted to obtain more accurate calculation results.

In addition, to simulate the coexistence of rolling and sliding during actual operation, the periodic step function is used to set the angular velocity of the thread pair, which is given as follows:

$$\omega' = (-1)^{[2t/T]} \omega \quad (39)$$

where ω' is the angular velocity in the simulation, t is the simulation time, T is the period, the symbol $[\]$ is the rounding symbol, and ω is the angular velocity under the test condition.

The angular velocity of the screw is 300 rpm (i.e., 31.4 rad/s), and the angular velocity of the roller can be calculated as -28.4 rad/s, while the sliding-rolling ratio is 0.3. The simulation time $t = 0.03$ s, and the period $T = 0.01$ s. The variation curves of the angular velocities of the screw and the roller with time are shown in Fig. 11 and Fig. 12, respectively. In Figs. 11 and 12, every change in the angular velocity direction is defined as one cycle of the thread pair, i.e., there are six wear cycles.

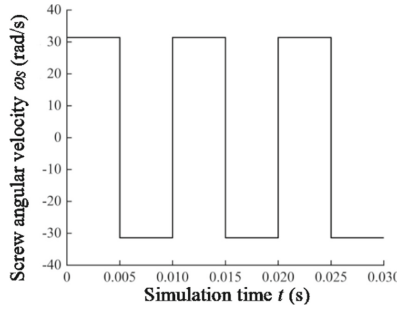


Fig. 11. The variation curve of the screw angular velocity

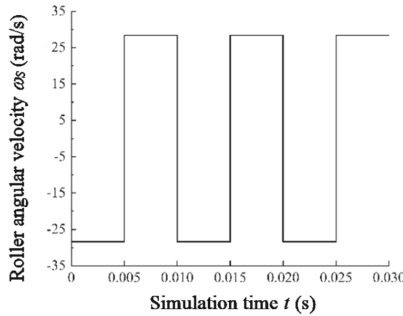


Fig. 12. The variation curve of the roller angular velocity

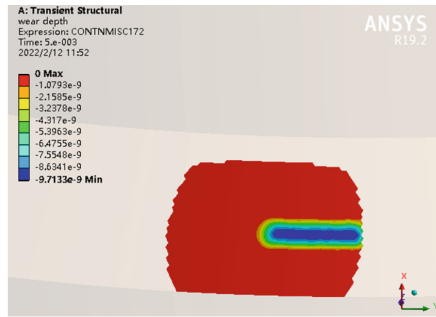
3.2 Model Validation and FE Simulation Results

The simulation results of the wear depth for different wear cycles are shown in Fig. 13.

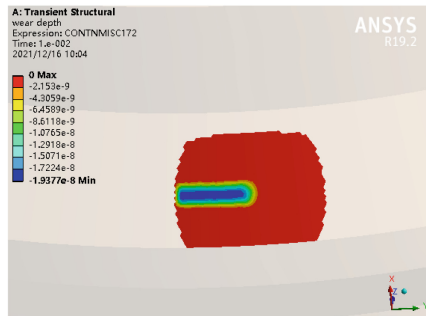
Figures 13 show that the wear shape from the simulation is a wear band, which is close to the theoretical analysis and test results. The wear depth presents a gradient distribution, the wear amount at the center of the contact ellipse is the largest, the wear amount far from the center of the contact ellipse decreases in turn. This is because the wear depth increases gradually with the increase in wear cycles and the contact stress distribution. The maximum wear depth after six wear cycles can be extracted from the simulation results.

Equation (11) and Eq. (12) can be used to calculate the wear depth and wear volume, and the results are used as analytical solutions to compare with the numerical solutions. The wear depth and wear volume from the numerical solution and the analytical solution are compared in Table 7 and Table 8.

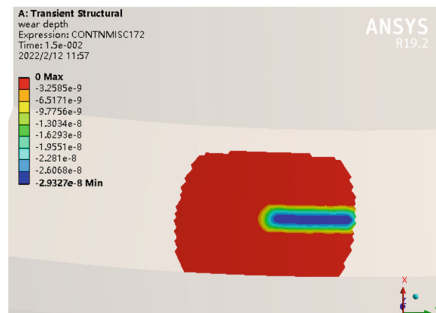
As shown in Table 7 and Table 8, the relative error between the two sets of results is less than 9%, and the error is acceptable. Therefore, the analytical wear model proposed in this paper is valid and can be used for wear analysis of thread pair in the PRSM. The wear depth and wear volume tend to increase linearly with increasing wear cycles.



(a) The wear depth under first cycle ($t=0.005s$)

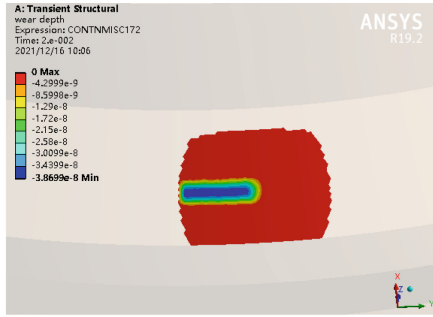


(b) The wear depth under 2 numbers of cycles ($t=0.01s$)

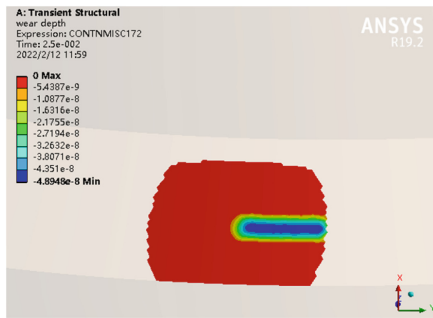


(c) The wear depth under 3 numbers of cycles ($t=0.015s$)

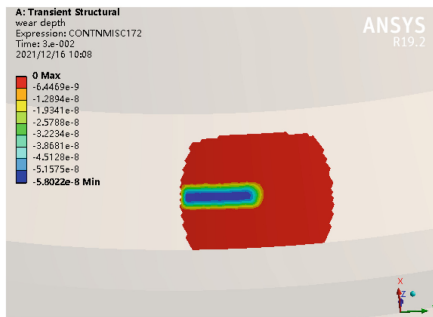
Fig. 13. The simulation results of the wear depth for different wear cycles



(d) The wear depth under 4 numbers of cycles ($t=0.02s$)



(e) The wear depth under 5 numbers of cycles ($t=0.025s$)



(f) The wear depth under 6 numbers of cycles ($t=0.03s$)

Fig. 13. (continued)

With the increase in wear cycles, the relative error also increases gradually. This is because the contact stress in the actual contact changes with the variation in movement and wear, i.e., the dynamic change in contact stress is not considered in the theoretical calculation. Thus, the contact stress is calculated as a constant. In contrast, the finite element simulation can automatically adjust the benchmark of the surface morphology and update the geometric morphology of the contact surface according to the changes in the geometry of the contact surface. Table 7 and Table 8 show that the analytical

Table 7. Comparison of cumulative wear depth between the analytical solution and numerical solution under different wear cycles

Cumulative Wear depth ($\times 10^{-8}$ mm)	Wear cycles					
	1	2	3	4	5	6
Numerical solution	0.97	1.94	2.93	3.87	4.89	5.80
Analytical solution	1.06	2.12	3.17	4.23	5.29	6.35
Relative error	8.5%	8.5%	7.6%	8.5%	7.6%	8.7%

Table 8. Comparison of cumulative wear volume between the analytical solution and numerical solution under different wear cycles

Cumulative Wear volume ($\times 10^{-8}$ mm)	Wear cycles					
	1	2	3	4	5	6
Numerical solution	4.81	9.54	14.23	18.96	23.69	28.48
Analytical solution	5.15	10.30	15.45	20.60	25.76	30.90
Relative error	6.6%	7.4%	7.9%	8.0%	8.0%	7.8%

solutions are larger than the numerical solutions. By comparing the contact area, the meshing size causes the contact area in the FE model to be slightly larger than that of the analytical model, resulting in a smaller numerical solution.

4 Conclusions

In this paper, based on the point contact characteristics of helical surfaces, the adhesive wear model of the thread pair in a PRSM is developed based on adhesive wear theory. To more accurately calculate the wear depth and the wear volume of the screw raceway in the whole effective stroke, a test rig of the thread wear is established to obtain the values of the stress index and speed index and further deduce the area coefficient to reflect the real wear condition of the thread pair. The stress index and velocity index are obtained by fitting the wear rate under different axial loads and at different angular velocities. To verify the correctness of the wear model, the transient dynamic simulation of the thread wear based on the FE model is performed. The relative error is less than 9%, which indicates the wear model proposed in this paper is correct and can be used to forecast the thread wear of the PRSM. The presented work has significance in the wear behavior of the PRSM and is benefit to enhance its positional accuracy and carrying capacity.

Authors' Contributions. SM: conceptualization; methodology; writing-original draft. QX: data analysis; visualization; writing-original draft. CL: investigation; formal analysis. JZ: validation; writing-editing. GL: writing-review & editing. All authors read and approved the final manuscript.

References

1. Habibi, S., Roach, J., Luecke, G.: Inner-loop control for electromechanical (EMA) flight surface actuation systems. *J. Dyn. Syst. Meas. Control.* **130**(5), 51002–51013 (2008)
2. Karam, W., Mare, J.C.: Modelling and simulation of mechanical transmission in roller-screw electromechanical actuators. *Aircr. Eng. Aerosp. Technol.* **81**(4), 288–298 (2009)
3. Biju Prasad, B., Biju, N., Radhakrishna Panicker, M.R.: High redundancy electromechanical actuator for thrust vector control of a launch vehicle. *Aircr. Eng. Aerosp. Technol.* **91**(8), 1122–1132 (2019)
4. Deng, Q.: Applications status of on planetary roller screw electric cylinder. *Ship Eng.* **39**(1), 143–146 (2017)
5. Auregan, G., Fridrici, V., Kapsa, P., Rodrigues, F.: Experimental simulation of rolling-sliding contact for application to planetary roller screw mechanism. *Wear* **332–333**, 1176–1184 (2015)
6. Auregan, G., Fridrici, V., Kapsa, P., Rodrigues, F.: Wear behavior of martensitic stainless steel in rolling-sliding contact for planetary roller screw mechanism: study of the WC/C solution. *Tribol. Online* **11**(2), 209–217 (2016)
7. Xie, Z.J., Xue, Q.H., Wu, J.Q., Gu, L., Wang, L.Q., Song, B.Y.: Mixed-lubrication analysis of planetary roller screw. *Tribol. Int.* **140**, 105883–105889 (2019)
8. Zhou, G.W., Zhang, Y.H., Wang, Z.Z., Pu, W.: Analysis of transient mixed elastohydrodynamic lubrication in planetary roller screw mechanism. *Tribol. Int.* **163**, 107158–107212 (2021)
9. Sandu, S., Biboulet, N., Nelias, D., Abevi, F.: An efficient method for analyzing the roller screw thread geometry. *Mech. Mach. Theory* **126**, 243–264 (2018)
10. Sandu, S., Biboulet, N., Nelias, D., Abevi, F.: Analytical prediction of the geometry of contact ellipses and kinematics in a roller screw versus experimental results. *Mech. Mach. Theory* **131**, 115–136 (2019)
11. Qiao, G., Liu, G., Ma, S.J.: Principal curvature calculation and contact characteristics analysis of the planetary roller screw mechanism. *J. Mech. Eng.* **56**(21), 140–148 (2020). (in Chinese)
12. Velinsky, S.A., Chu, B., Lasky, T.A.: Kinematics and efficiency analysis of the planetary roller screw mechanism. *J. Mech. Des.* **131**(1), 011016–011018 (2009)
13. Jones, M.H., Velinsky, S.A.: Kinematics of roller migration in the planetary roller screw mechanism. *J. Mech. Des.* **134**(6), 61006–61016 (2012)
14. Ma, S.J., Liu, G., Fu, X.J., Tong, R.T.: Rolling-sliding characteristics of planetary roller screw considering elastic deformation. *J. Southeast Univ. (Nat. Sci. Edn.)* **45**(3), 461–468 (2015). (in Chinese)
15. Abevi, F., Daidie, A., Chaussumier, M., Sartor, M.: Static load distribution and axial stiffness in a planetary roller screw mechanism. *J. Mech. Des.* **138**(1), 012301–012311 (2016)
16. Zhang, W.J., Liu, G., Ma, S.J., Tong, R.T.: Load distribution over threads of planetary roller screw mechanism with pitch deviation. *Proc. Inst. Mech. Eng. Part C J. Mech. Eng. Sci.* **233**(13), 1–14 (2019)
17. Zhang, X.P., Shang, J.Z., Chen, X., Zhang, C.H., Wang, Y.S.: Wear-life models for angular contact spherical plain bearing under different load types. *Appl. Mech. Mater.* **344**, 3–7 (2013)
18. Jones, M.H., Velinsky, S.A.: Contact kinematics in the planetary roller screw mechanism. *J. Mech. Des.* **135**(5), 01003–51010 (2013)
19. Ma, S.J., Wu, L.P., Fu, X.J., Li, Y.J., Liu, G.: Modelling of static contact with friction of the threaded surfaces in a planetary roller screw mechanism. *Mech. Mach. Theory* **139**, 212–236 (2019)

Open Access This chapter is licensed under the terms of the Creative Commons Attribution-NonCommercial 4.0 International License (<http://creativecommons.org/licenses/by-nc/4.0/>), which permits any noncommercial use, sharing, adaptation, distribution and reproduction in any medium or format, as long as you give appropriate credit to the original author(s) and the source, provide a link to the Creative Commons license and indicate if changes were made.

The images or other third party material in this chapter are included in the chapter's Creative Commons license, unless indicated otherwise in a credit line to the material. If material is not included in the chapter's Creative Commons license and your intended use is not permitted by statutory regulation or exceeds the permitted use, you will need to obtain permission directly from the copyright holder.

